JOURNAL OF APPLIED PHYSICS **107**, 024101 (2010)

Piezoelectric $Pb(Zr_{0.52}Ti_{0.48})O_3$ thin films on single crystal diamond: Structural, electrical, dielectric, and field-effect-transistor properties

Meiyong Liao,[1,a)] Yasuhito Gotoh,[2] Hiroshi Tsuji,[2] Kiyomi Nakajima,[3] Masataka Imura,[1] and Yasuo Koide[1,3]
[1]*Sensor Materials Center, National Institute for Materials Science (NIMS), 1-1 Namiki, Tsukuba, Ibaraki 305-0044, Japan*
[2]*Department of Electronic Science and Engineering, Kyoto University, Nishikyo Ku, Kyoto 615-8510, Japan*
[3]*Nano-Innovation Center (NICe), National Institute for Materials Science (NIMS), 1-1 Namiki, Tsukuba, Ibaraki 305-0044, Japan*

(Received 27 August 2009; accepted 26 November 2009; published online 21 January 2010)

The combination of piezoelectric materials and single crystal diamond offers the opportunity for the development of multifunctional micromachined devices under extreme conditions. In this work, the authors report the structural, electrical, optical, and dielectric properties of $Pb(Zr_{0.52},Ti_{0.48})O_3$ (PZT) thin films integrated on single crystal diamond (100) substrates. The corresponding field effect transistor based on the metal-piezoelectric-insulator-semiconductor (MPIS) structure was fabricated on a homoepitaxial p-type diamond layer grown on a type-Ib diamond substrate. Different intermediate layers were deposited on single diamond substrates prior to the PZT films growth in order to achieve the best polarization properties. It was observed that the utilization of an Al_2O_3 buffer layer followed by a $SrTiO_3$ seed layer favored the formation of a single perovskite PZT phase. Transmission electron diffraction patterns revealed that the PZT films included an initial layer at the $SrTiO_3$/PZT interface followed by a well crystallized layer. The PZT film grown on $SrTiO_3/Al_2O_3$/diamond exhibited much better in-plane polarization than that of the PZT film on Al_2O_3/diamond. The photoresponse behavior revealed that carriers trapping effect was trivial in the PZT film. The channel electrical conductivity of the MPIS field effect transistor was successfully modulated by the gate bias. © *2010 American Institute of Physics*. [doi:10.1063/1.3282706]

I. INTRODUCTION

Diamond is an attractive material for micro- or nanoelectromechanical system (M/NEMS). It possesses the highest acoustic velocity among all the materials, very high thermal conductivity, exceptional wear resistance, and chemical inertness.[1] The electrical conductivity of diamond can be tailored from intrinsic insulator to conductor through doping. The M/NEMS actuators/resonators manufactured from diamond can overcome the drawbacks of silicon, which has relatively poor physical, chemical, and mechanical properties. For example, diamond resonator exhibited higher intrinsic vibration frequency than silicon in the same dimensional scale.[2] It was demonstrated that nanocrystalline diamond oscillators possessed high quality factors, which allowed the detection of mass loading with high sensitivity.[3] The rf microelectromechanical system (MEMS) switch using diamond was reported by virtue of its low or no stiction.[4] Despite the great progress in diamond MEMS, all the devices had been based on polycrystalline diamonds. The current achievement in microwave plasma chemical vapor deposition offers the possibility to use high quality single crystal diamond for M/NEMS devices. Such a related research, however, has not been launched yet.

In order to develop diamond M/NEMS, the integration of piezoelectric materials on diamond is of prior importance. Lead zirconate titanate $Pb(Zr_xTi_{1-x})O_3$ (PZT) is an excellent piezoelectric material with high electromechanical coupling coefficient and electrical polarization. The integration of PZT on diamond provides the opportunity of actuating with low voltage and sensing the displacement by using a diamond cantilever or bridge.[5] On the other hand, by combining the outstanding piezoelectric properties of PZT and the excellent semiconductor properties of diamond in a metal-piezoelectric-insulator-semiconductor (MPIS) structure, diamond field effect transistor (FET) can be utilized as MEMS pressure sensors under elevated temperatures.[6] However, no attempt has been reported on the diamond MPIS-FET up to now.

To carry out practical applications of single diamond to MEMS, comprehensive investigation on the structural, electrical, optical, ferroelectric, and related devices properties of the PZT films is urgently required. The purposes of this paper are twofold. The first is to understand the growth behavior of the PZT films on diamond. The second is to investigate the electrical, optical, and ferroelectric/piezoelectric properties for MEMS devices applications.

II. EXPERIMENTAL

The PZT films were deposited on single crystal diamond substrates by using a rf magnetron sputter apparatus (13.56 MHz) at ambient substrate temperatures. The single diamond substrates for the PZT growth include insulating type-Ib diamonds and boron-doped p-type diamond homoepitaxial layers grown on type-Ib diamond substrates. The p-type dia-

---

[a)] Electronic mail: meiyong.liao@nims.go.jp.

mond epilayers were grown by using a microwave plasma enhanced chemical vapor deposition (MPCVD) apparatus. The detailed MPCVD growth process can be found elsewhere.[7] The PZT target was $Pb(Zr_{0.52},Ti_{0.48})\ O_3$ with 99.9% above in purity. Before sputtering, the diamond substrates were cleaned in a boiling acid solution of $HNO_3:H_2SO_4=1:2$, and then, stirred in acetone and deionized water. Four types of intermediate layers on the diamond substrates were used for the deposition of PZT films: bare diamond, 15 nm thick Al_2O_3 buffer layer on diamond (Al_2O_3/diamond), 50 nm thick strontium titanate (STO) layer on diamond (STO/diamond), and 15 nm thick Al_2O_3 layer followed by a 25 or 50 nm thick STO layer on diamond (STO/Al_2O_3/diamond). The output rf-power during the PZT films and Al_2O_3 layers depositions was around 50 W, while a power of 100 W was applied for the deposition of the STO films. The Al_2O_3 and STO films were also grown at ambient temperatures. The sputtering chamber was evacuated down to 1.3×10^{-3} Pa as the background pressure. The working pressure was fixed at 1 Pa for all the sputter depositions. The feed gas for the sputtering was Ar with a 30 SCCM (SCCM denotes standard cubic centimeter per minute) flowing flux. Note that no oxygen was added during the deposition. The PZT films were thermally annealed at 650 °C for 3 min in an O_2 ambient. The thickness of the PZT films was around 400 nm.

The crystalline structure of the PZT films was identified by a Rigaku x-ray diffraction (XRD) system with a Cu $K\alpha$ x-ray source (wavelength of 0.154 nm). High resolution transmission electron microscopy (HRTEM) and selected area diffraction (SAD) were used to characterize the microstructure of the PZT films by using a JEOL JEM-2100F system with an acceleration voltage of 200 kV. The TEM specimen was fabricated by using a focused Ga^+ ion beam/scanning electron microscopy dual-beam system (SII Xvision200). The chemical bonding states were characterized by x-ray photoelectron spectroscopy (XPS) apparatus (Kratos AXIS 165 S) with monochromatized Al $K\alpha$ (1486.6 eV) radiation.

In order to measure the electrical, photoelectrical, and ferroelectric polarization properties of the PZT films, two tungsten carbide (WC) electrodes with interdigitated fingers (IDFs) were sputter-deposited on the PZT surface. This leads to that both the polarization and applied electric field are along the surface of the PZT layer, which can disclose the ferroelectric polarization of the PZT films on insulating substrates. The in-plane polarization was measured by using a P-LC100 ferroelectric test system (Radiant Technologies Inc.) at 50 Hz. The dissipation factor was measured at a bias of 5 V and different frequencies up to 1 MHz. The photoelectrical properties such as the bandgap and transient photocurrent behavior of the PZT film were characterized by using an Acton Research monochromator.

The MPIS-FET was fabricated on a p-type diamond layer grown on a type-Ib diamond substrate. A dry etching process was conducted for the formation of the diamond mesa structure. The insulating nature of the type-Ib diamond allows good electrical separation for the fabrication of MPIS-FET devices. The channel length and width were 140 and 400 μm, respectively. The electrodes for the source and gain were annealed Ti/WC. The gate included the PZT/STO/Al_2O_3 stack with an electrode of WC.

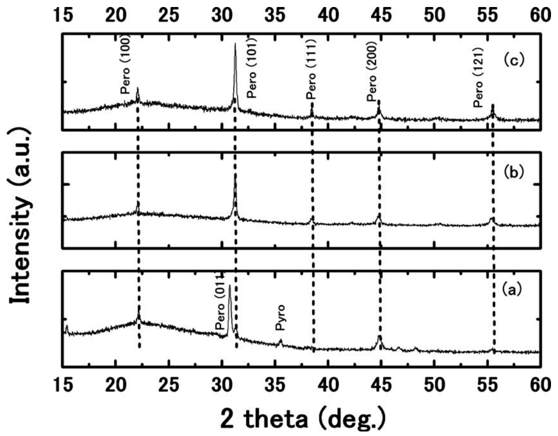

FIG. 1. Typical XRD patterns of the annealed PZT films deposited on (100) single crystal diamond substrates by using (a) Al_2O_3 buffer layer, (b) Al_2O_3 buffer layer and 25 nm thick STO seed layer, and (c) Al_2O_3 buffer layer and 50 nm thick STO seed layer.

III. RESULTS AND DISCUSSION

A. Crystalline structure and composition

All the as-deposited PZT films were amorphous despite the substrate types investigated. The PZT films directly grown on bare diamond and STO/diamond substrates maintained the amorphous state even after post annealing. Figure 1 shows the XRD patterns of the PZT films deposited on (a) Al_2O_3(15 nm)/diamond, (b) STO(50 nm)/Al_2O_3(15 nm)/diamond, and (c) STO(25 nm)/Al_2O_3(15 nm)/diamond substrates, respectively, after thermally annealing. No diamond peak was observed in the investigated range, indicating the good quality of the (100)-oriented single crystal. The PZT film deposited on the Al_2O_3/diamond substrate contains both perovskite and pyrochlore phases with the predominant perovskite phase. On the other hand, only a single ferroelectric phase appears on the STO/Al_2O_3/diamond substrate. This indicates that the STO layer enhances the nucleation of the perovskite PZT phase by lowering its crystallization temperature. This is reasonable since the crystal structure and lattice constant between STO and perovskite PZT are similar.[8] No difference in the structure between the PZT films with different STO thicknesses is observed. The failure of the formation of the perovskite PZT on STO/diamond after annealing suggests that Al_2O_3 is also requisite for achieving the ferroelectric phase. The Al_2O_3 layer is known to act as an efficient diffusion barrier between the element Pb and diamond.[9]

The cross-section TEM and SAD measurements were performed on the PZT film deposited on the STO (25 nm)/Al_2O_3(15 nm)/diamond substrate after annealing, as shown in Fig. 2. From the cross-section TEM image, the layered structure can be clearly observed. The SAD patterns were taken from the bottom diamond substrate to the top PZT layer step by step, as illustrated in Figs. 2(b)–2(d), which correspond to the diffraction patterns from the dia-

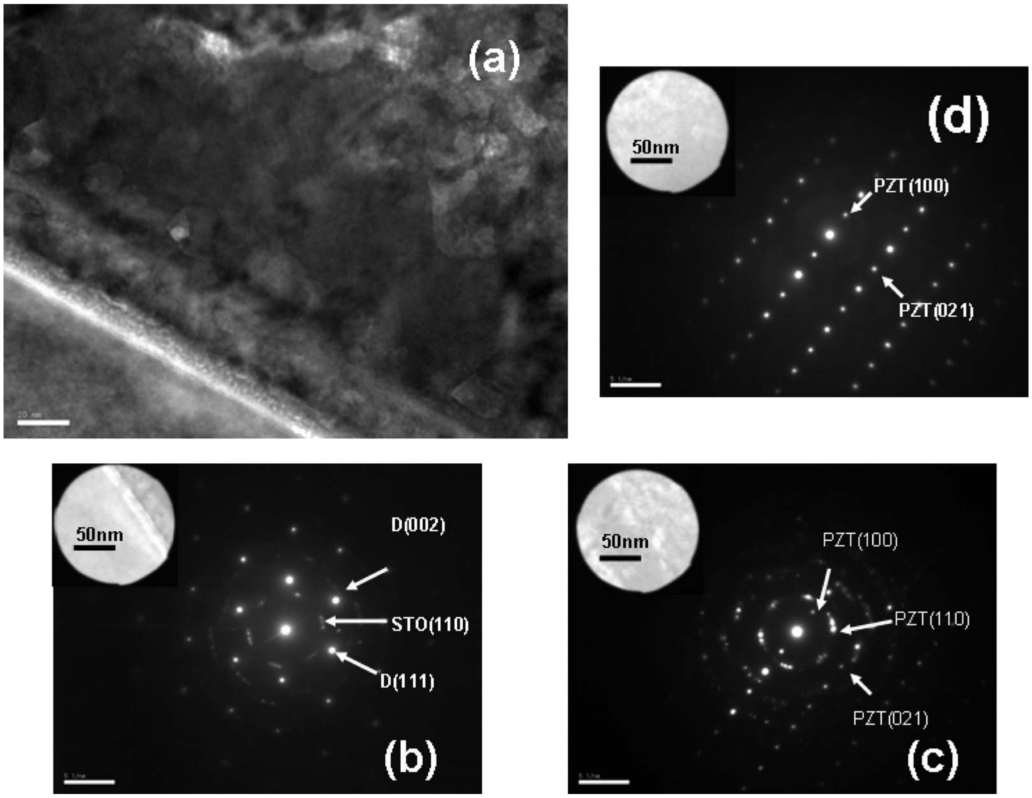

FIG. 2. (a) Cross-section TEM image of the PZT/STO/Al_2O_3/diamond, (b) SAD pattern from the region of diamond/Al_2O_3/STO, (c) SAD pattern from the PZT layer near to the STO layer, and (d) SAD pattern from the PZT layer far from the STO layer.

mond substrate to the STO layer, the PZT layer adjacent to the STO layer, and the PZT layer far from the STO layer. The electron beam was parallel to the diamond [110] direction. It is observed that the Al_2O_3 layer is amorphous and the STO layer is nearly polycrystalline. No appearance of XRD peaks from the STO layer is probably due to that the signal from the STO is too weak (or it is too thin) to be detected by the facility. The SAD patterns indicate that the initial PZT layer on STO exhibits nearly polycrystalline nature, as shown in Fig. 2(c) and that the subsequent PZT grains show good crystallinity, as revealed in Fig. 2(d).

Figure 3(a) shows the HRTEM image containing the interfaces of STO/Al_2O_3 and PZT/STO. It suggests a good expitaxial relationship between STO and PZT, as can be seen from the fast-Fourier-transform (FFT) image. Figure 3(b) is the HRTEM image from one PZT grain far away from the PZT/STO interface, indicating the good crystallinity of the PZT film.

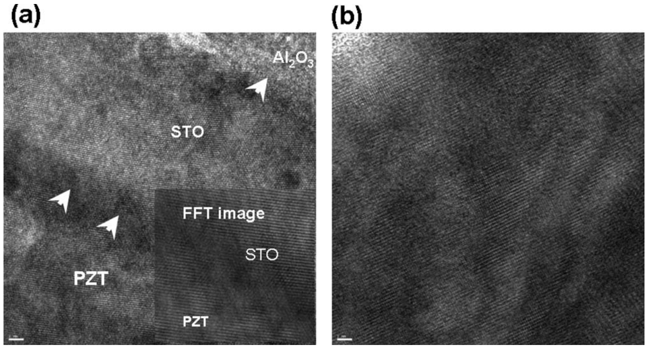

FIG. 3. (a) HRTEM image including the interfaces of PZT/STO and STO/Al_2O_3 and (b) HRTEM image from a PZT grain. The arrows show the interface. The inset in (a) is the FFT image of the PZT/STO interface.

The formation of the perovskite PZT phase was confirmed further by measuring the chemical bonding states of Pb 4*f*, Ti 2*p*, and Zr 3*d* of a typical annealed PZT film deposited on the STO/Al_2O_3/diamond substrate by using XPS. The peak positions in the XPS spectra were calibrated by referring to the C 1*s* 284.5 eV peak due to air contamination. To remove the influence of air exposure, the film surface was etched by energetic Ar ions in the chamber of the XPS apparatus. Figure 4 illustrates the XPS spectra of (a) Ti 2*p*, (b) Zr 3*d* after Ar etching, and of (c) Pb 4*f* before and after etching. The measured peak positions for Zr $3d_{5/2}$ and Zr $3d_{3/2}$ are 181.9 and 184.2 eV, respectively, and for Ti $2p_{3/2}$ and Ti $2p_{1/2}$ are 463.8 and 458.1 eV, respectively. No significant difference is found for these peaks before and after Ar etching. These values are consistent with those reported on perovskite PZT film.[10,11] On the other hand, the Pb 4*f* spectra exhibit a complex behavior. Before etching, only one spin-orbit doublet is observed with peak positions of Pb $4f_{7/2} = 138.1$ eV and Pb $4f_{5/2} = 143$ eV due to the perovskite PZT phase. After etching, an additional spin-orbit doublet appears with peak positions of Pb $4f_{7/2} = 136.1$ eV and Pb $4f_{5/2} = 141.1$ eV. This doublet can be attributed to metallic Pb. The presence of metallic Pb is due to the Ar ion bombardment during etching, causing preferential sputtering of oxygen in the PZT film. The segregation of Pb was also ob-

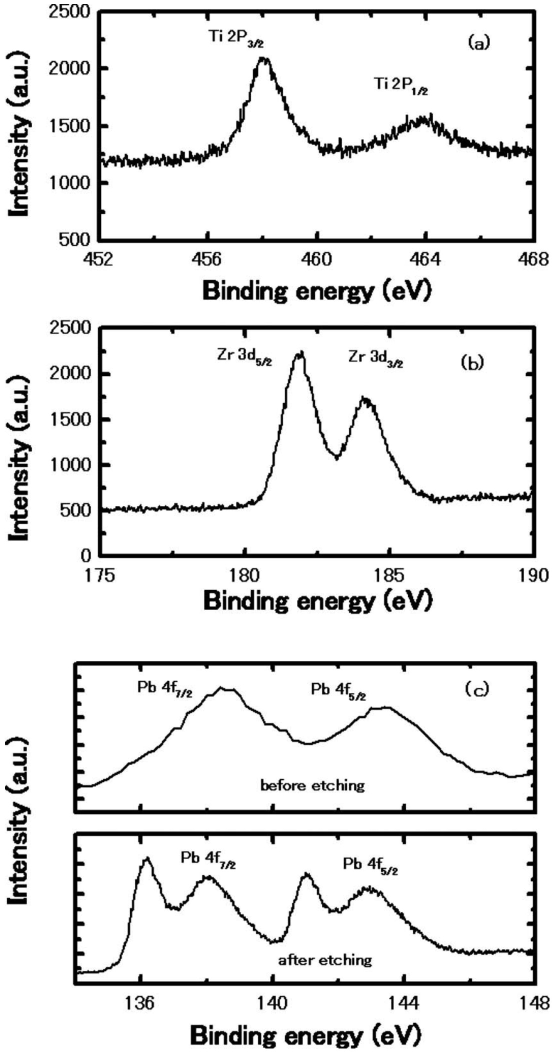

FIG. 4. XPS spectra of (a) Ti 2*p*, (b) Zr 3*d* after etching, and (c) Pb 4*f* before and after etching.

served by other researchers.[10] The XPS survey further supports the single perovskite phase nature of the annealed PZT film on STO/Al_2O_3/diamond.

B. Dielectric properties

Figure 5 illustrates the polarization versus applied electric field of the annealed PZT film on STO/Al_2O_3/diamond compared with that of the film on Al_2O_3/diamond. The electrodes configuration for the polarization measurement is illustrated in Fig. 5(a). The utilization of planar electrodes on the film surface leads to that the applied electric field is in the transverse direction, corresponding to the d_{33} mode. It should be mentioned that the previous work on polycrystalline/nanocrystalline diamond used the conventional sandwich structure, in which a bottom electrode was required.[5,12] The d_{33} mode in the present study simplifies the fabrication process for diamond MEMS devices and avoids the difficulty in the growth of single crystal diamond on foreign substrates. As revealed in Fig. 5(b), the dielectric hysteresis is observed for both films, disclosing that in-plane polarization occurs in the PZT films.[13] To calculate the remanent polarization ($2P_r$) and coercive electric field, the area (1.06×10^{-5} cm^2) switched was assumed to be the product of the electrode fingers length and PZT film thickness. We also consider that the electric field is uniform across the electrode gap. Therefore, the typical remanent polarization and the coercive electric field for the PZT film on STO/Al_2O_3/diamond are around 40 $\mu C/cm^2$ and below than 40 kV/cm, respectively, upon an applied electric field of 100 kV/cm. This remanent polarization is two times larger, and the coercive field is lower than those of the PZT film on Al_2O_3/diamond. As disclosed by the structural analysis, the degradation of the ferroelectric properties for the PZT film on the Al_2O_3/diamond is due to the appearance of pychlore phase. It is demonstrated that the PZT film with excellent in-plane polarization can be achieved on single crystal diamond.

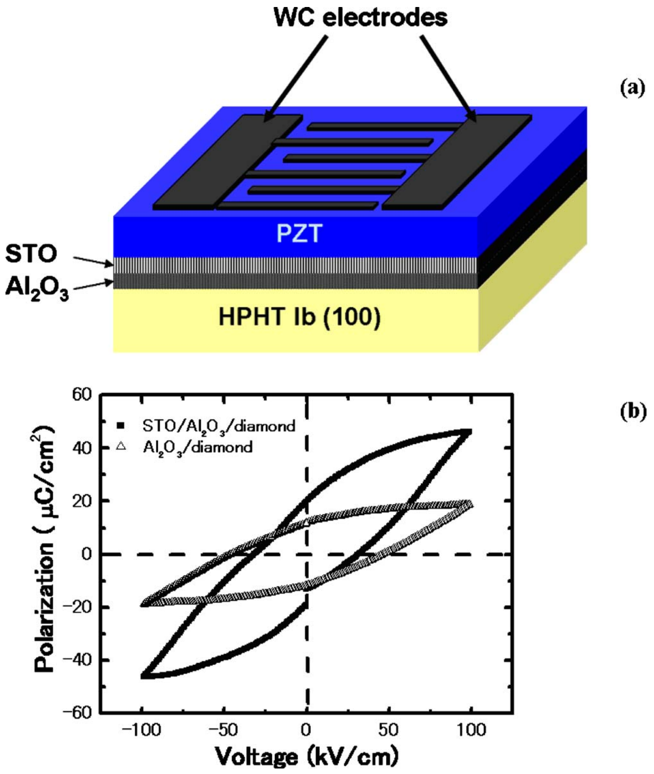

FIG. 5. (Color online) (a) IDF electrodes configuration for the electrical polarization measurements and (b) the corresponding dielectric hysteresis loop at 100 kV/cm and 50 Hz for the PZT films on Al_2O_3/diamond and STO/Al_2O_3/diamond, respectively.

The dissipation factor (tan δ) or dielectric loss of the PZT/STO/Al_2O_3/diamond capacitor based on the surface IDF electrodes is shown in Fig. 6, which was measured at different frequencies at a bias of 5 V. The dissipation factor is around 0.034 at 10 KHz and reduces to 0.027 for the frequencies higher than 50 kHz. These values are very low and comparable with that of the PZT film fabricated using a $LaNiO_3$ intermediate layer on a glass substrate.[14] The low loss is considered to be due to the good control of the stoichiometric composition.[14] This is consistent with the XPS results.

C. Electric and optical properties

The dark electrical conductivity and the photocurrent spectrum were measured by using the device structure de-

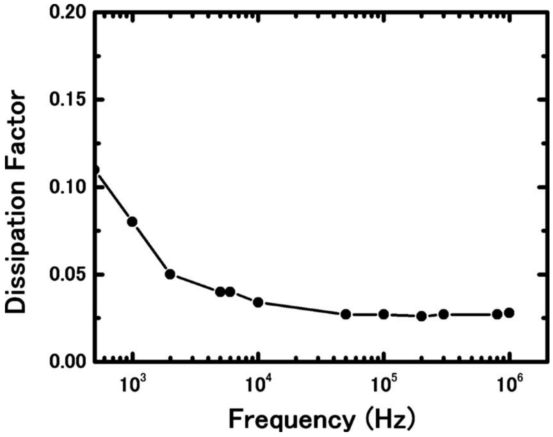

FIG. 6. Dissipation factor for a PZT/STO/Al_2O_3/diamond capacitor using surface IDF electrodes.

scribed in Fig. 5(a). It discloses that the dark current of the PZT film is as low as 10^{-13} A for a voltage of 32 V at least. Therefore, the PZT film has good insulating property. To use the PZT film in MPIS-FET pressure sensors, the energy band information should be disclosed. Shown in Fig. 7(a) is the normalized photocurrent spectrum of the PZT film on STO/Al_2O_3/diamond. The bandgap of the PZT film was deduced from this spectrum, which is typically around 3.7 eV.[15] The fast response of the PZT film to the 330 nm UV light, depicted in Fig. 7(b), reveals that the carrier trapping effect in the surface region of the PZT film or at the metal/PZT interface can be neglected.[16]

D. Metal-piezoelectric-insulator-diamond FET

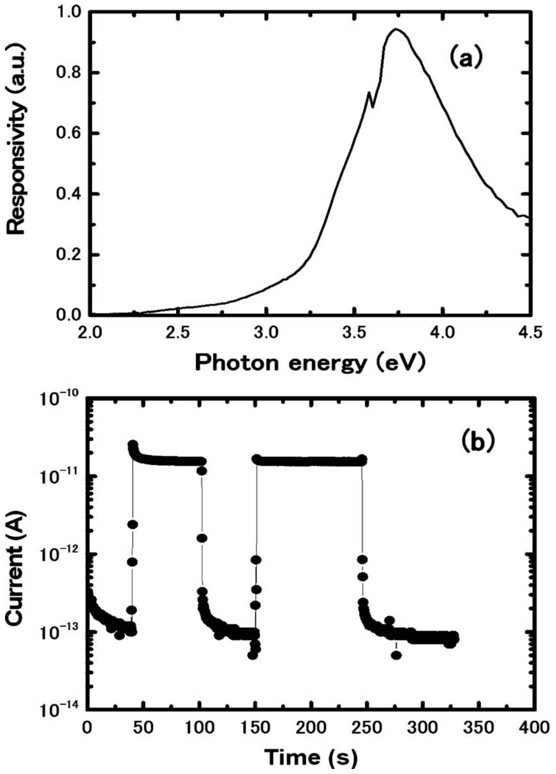

FIG. 7. (a) Photocurrent spectrum of the PZT film using IDF electrodes and (b) time response to 330 nm UV light.

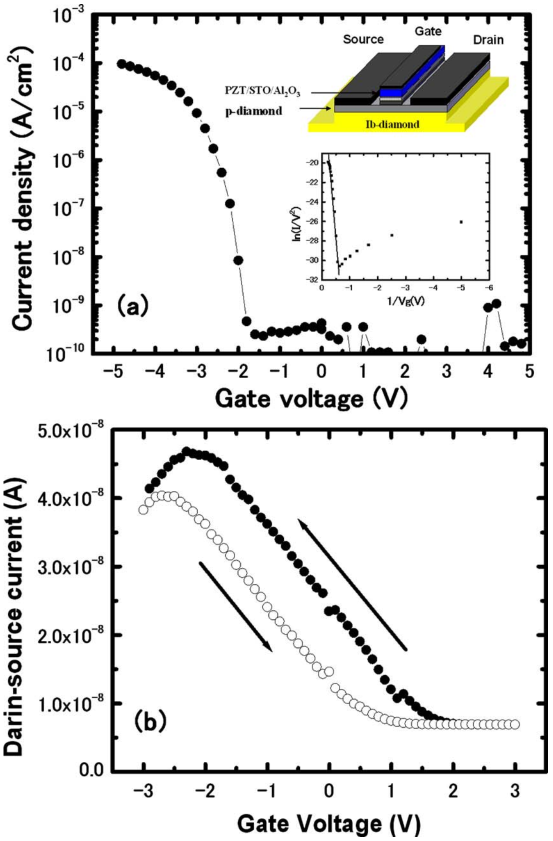

FIG. 8. (Color online) (a) Gate voltage and source current characteristics of the PZT/STO/Al_2O_3 on p-diamond with the drain suspended and (b) drain-source current dependence on the gate voltage at a drain-source voltage of 5 V.

The boron-doped single crystal diamond epilayer grown on a type-Ib diamond substrate was utilized for the fabrication of the MPIS-FET. The boron concentration in the epilayer is around 10^{17} cm^{-3}. The device structure is illustrated in the inset of Fig. 8(a). The leakage current of the MPIS structure was measured by biasing the gate and grounding the source with the drain suspended. As shown in Fig. 8(a), the leakage current at reverse biases (positive bias on the gate electrode) is at the noise level of the picoammeter (10^{-13} A) for the MPIS, similar to the Schottky barrier diode. At negative gate biases (or forward direction), the leakage current is around 10^{-4} A/cm^2 at −5 V, which is comparable with that of the PZT film grown on a silicon substrate using a Y_2O_3 insulating layer.[17] The I-V characteristic at high negative biases was fitted with the field or tunneling emission theory, which can be expressed as[18]

$$I \propto V^2 \exp(-b/V), \tag{1}$$

where b is a constant. In the inset of Fig. 8(a), the plot of ln (I/V^2) versus 1/V is almost linear, revealing that the leakage current is dominated by tunneling emission.

The gate voltage (V_g) versus drain-source current (I_{ds}) was measured at a drain-source voltage (V_{ds}) of 5 V. The gate voltage was first swept from 3 to −3 V, then from −3 to 3 V. The result is shown in Fig. 8(b), which demonstrates that the drain-source current can be modulated by the gate voltage. The overall V_g-I_{ds} curves disclose a counterclockwise hysteresis, which is related to charge traps. The appearance of the V_g-I_{ds} hysteresis and its asymmetrical shape reveal that charges are injected mainly from one electrode. In addition, the reduction of I_{ds} smaller than -2 V is due to the increase in the gate-source leakage current. These are consistent with the I-V characteristics, shown in Fig. 8(a).

From the transient photocurrent behavior in Fig. 7(b), charge traps do not exist near the PZT surface or at the metal/PZT interface. Therefore, the shift of V_g toward the left hand with the sweep voltage from -3 to 3 V indicates that charges are trapped at the interfaces of the oxide layers. The origin for the V_g-I_{ds} counterclockwise hysteris is possibly due to holes trapping at the Al_2O_3/diamond interface, or the deficiency of Pb in the initial PZT layer near the STO layer due to interface diffusion.[9]

The utilization of the MPIS-FET to MEMS pressure sensors requires that the channel conductivity should be controlled by the gate bias, which is really achieved in the present work. The external pressure applied on the gate will induce a polarization of the PZT film, consequently, an additional bias on the gate. Therefore, the channel electrical conductivity of the MPIS-FET will be modified by the external pressure despite the existence of interfaces traps. The present work provides the potential for the development of MEMS pressure sensors based on the diamond MPIS-FET operating at elevated temperatures.

IV. SUMMARY

The structural, electrical, optical, polarization, and the MPIS-FET properties of the PZT films deposited by rf-sputtering on single crystal diamond substrates were studied. The effect of various intermediate layers on the PZT film growth was investigated in order to achieve the best in-plane dielectric properties. Under the same fabrication process, an Al_2O_3 buffer layer followed by a $SrTiO_3$ seed layer was found to be requisite for the formation of a single perovskite PZT phase. The PZT film contained an initial layer at the interface of PZT/STO with relatively poor crystallinity followed by a top layer with good crystallinity. The PZT film on STO/Al_2O_3/diamond showed excellent ferroelectric properties for M/NEMS applications, which was better than that of the PZT film on Al_2O_3/diamond. The MPIS-FET using the boron-doped single crystal diamond epilayer on the type-Ib diamond substrate was fabricated. It was revealed that the channel electrical conductivity of the FET was successfully modulated by the gate voltage. The integration of PZT films on diamond provides the way for developing micromachined devices by using the extreme mechanical and semiconductor properties of diamond.

ACKNOWLEDGMENTS

This work was partially supported by Grant-in-Aid for Young Scientists (Grant No. 21760267) from the Ministry of Education, Culture, Sports, Science, and Technology. M.Y.L is indebt to Yoshihiro Nemoto (MANA, NIMS) for his technical support in TEM.

[1] J. Kusterer, A. Lüker, P. Herfurth, Y. Men, W. Ebert, P. Kirby, M. O'Keefe, and E. Kohn, Diamond Relat. Mater. **17**, 1429 (2008).
[2] N. Sepulveda, D. Aslam, and J. P. Sullivan, Diamond Relat. Mater. **15**, 398 (2006).
[3] M. Imboden, P. Mohanty, A. Gaidarzhy, J. Rankin, and B. W. Sheldon, Appl. Phys. Lett. **90**, 173502 (2007).
[4] Y. Gurbuz, O. Esame, I. Tekin, W. P. Kang, and J. L. Davidson, Solid-State Electron. **49**, 1055 (2005).
[5] S. Srinivasan, J. Hiller, B. Kabius, and O. Auciello, Appl. Phys. Lett. **90**, 134101 (2007).
[6] Y. R. Wu and J. Singh, Appl. Phys. Lett. **85**, 1223 (2004).
[7] M. Y. Liao, Y. Koide, and J. Alvarez, Appl. Phys. Lett. **87**, 022105 (2005).
[8] B. Xiao, V. Avrutin, H. Liu, U. Ozgur, H. Morkoc, and C. Lu, Appl. Phys. Lett. **93**, 052913 (2008).
[9] M. Y. Liao, M. Imura, X. S. Fang, K. Nakajima, G. C. Chen, and Y. Koide, Appl. Phys. Lett. **94**, 242901 (2009).
[10] J. Zhu and L. Lu, J. Appl. Phys. **95**, 241 (2004).
[11] C. H. Park, M. S. Won, C. S. Lee, W. H. Cha, and Y. G. Son, J. Electroceram. **17**, 619 (2006).
[12] T. Shibata, K. Unno, E. Makino, and S. Shimada, Sens. Actuators, A **114**, 398 (2004).
[13] B. Xu, Y. Ye, L. E. Cross, J. J. Bernstein, and R. Miller, Appl. Phys. Lett. **74**, 3549 (1999).
[14] K. K. Uprety, L. E. Ocola, and O. Auciello, J. Appl. Phys. **102**, 084107 (2007).
[15] D. Tiwari, S. Dunn, and Q. Zhang, Mater. Res. Bull. **44**, 1219 (2009).
[16] M. Y. Liao, Y. Koide, J. Alvarez, M. Imura, and J. P. Kleider, Phys. Rev. B **78**, 045112 (2008).
[17] W. C. Shih, P. C. Juan, and J. Y. Lee, J. Appl. Phys. **103**, 094110 (2008).
[18] S. M. Sze, *Physics of Semiconductor Devices*, 2nd ed. (Wiley, New York, 1981).